Magnetic textures and singularities in ferri/ferromagnetic multilayers

J. Hermosa,[1] A. Hierro-Rodríguez,[1,2] C. Quirós,[1,2] L. M. Álvarez-Prado,[1,2] A. Sorrentino,[3] R. Valcárcel,[3] S. Rehbein,[4] E. Pereiro,[3] J. I. Martín,[1,2] M. Vélez,[1,2] and S. Ferrer[3]

[1] Departamento de Física, Universidad de Oviedo, 33007 Oviedo, Spain
[2] CINN (CSIC – Universidad de Oviedo), 33940 El Entrego, Spain
[3] ALBA Synchrotron, 08290 Cerdanyola del Vallès, Spain
[4] Helmholtz Zentrum Berlin für Materialien und Energie GmbH, 12489 Berlin, Germany

Abstract

The stacking of ferrimagnetic and ferromagnetic films leads to a competition between magnetic interactions that can stabilize Bloch points and other singularities at the interfaces. In this work, $Gd_xCo_{1-x}/NdCo_5/Gd_yCo_{1-y}$ trilayers, with different thicknesses, have been prepared. By tuning the stoichiometry of the Gd-Co outer layers, the Co magnetic sublattice dominates in one layer, whereas the opposite side is Gd dominated. In this way, in-depth magnetization domain walls can be created due to the balance between exchange and magnetostatic interactions. In addition, the weak perpendicular magnetic anisotropy of the Nd-Co central layer induces a stripe domain pattern, supporting the formation of Bloch points, meron-like textures, and vortex-antivortex pairs. The interaction between both types of structures, in-depth domain walls and magnetic singularities, has been studied by a combination of macroscopic Magneto-Optical Kerr Effect and Vibrating Sample Magnetometry measurements with microscopic Magnetic Force Microscopy and element selective magnetic Transmission soft X-ray Microscopy imaging. The results confirm marked changes in the magnetic properties of the trilayers, as compared with those single $NdCo_5$ films, and the formation of complex magnetic textures, associated with partial magnetization reversal, where magnetic singularities are formed.

Keywords: ferrimagnetic/ferromagnetic multilayers, rare earth – transition metal alloys, transmission X-ray microscopy

1. Introduction

Three dimensional nanoscale magnetic systems, and the magnetic textures and singularities associated to them, are attracting strong attention due to their potential applications in technological fields like sensing, actuating, data storage, and Internet of Things development [1]. Accordingly, several characterization tools have been recently developed to further understand the details of complex three dimensional nanoscale magnetic configurations [2-6]. These textures can nucleate in magnetic materials as a result of the competition between collinear Heisenberg exchange, non-collinear Dzyaloshinskii-Moriya (DM) exchange, magnetostatic, Zeeman and anisotropy interactions. Amorphous Rare Earth (RE) – Transition Metal (TM) alloys are very adequate for this goal, as they present a rich variety of magnetic configurations that, in addition, can be controlled by tuning composition and temperature [7-10].

In this context, amorphous RE-TM ferromagnetic materials with weak perpendicular magnetic anisotropy (WPMA), like $NdCo_5$, show stripe domain patterns [11] providing out-of-plane components of magnetization which, in combination with in-plane

anisotropy layers, have been shown to form magnetic singularities like Bloch points [4,12], meron-like textures [4,12-14], and vortex-antivortex pairs [15] in the vicinity of stripe domain dislocations.

On the other hand, in-depth interface domain walls can be tuned by adjusting composition and temperature in some amorphous RE-TM systems [16,17]. This is the case of Gd-Co ferrimagnetic multilayers which have a collinear antiferromagnetic exchange coupling interaction between Co and Gd magnetic moments [18], so that they can develop in-depth domain walls in multilayered systems [19]. In addition, skyrmionic textures have been recently observed in ferrimagnetic amorphous RE-TM alloys [20,21], which show inhibition of skyrmion Hall effect [22], and high speed domain wall motions [21,23].

In this work, magnetic configurations obtained when combining ferromagnetic and ferrimagnetic layers with interface domain walls are studied. These systems are very interesting for their potential use in information technologies [24]. If one of these layers has WPMA, providing three dimensional components of the magnetization, and the other has competing exchange interactions leading to in-depth domain walls, non-trivial three dimensional magnetic textures are formed where magnetic singularities can be stabilized. A recent report has shown interesting results combining a central ferrimagnetic multilayer with external symmetric ferromagnetic multilayers with relevant non-collinear exchange DM interactions leading to the coexistence of complete and partial tubular skyrmions [25]. In the work presented here a different approach is used, as a central ferromagnetic layer, with weak perpendicular magnetic anisotropy and significant magnetostatic effects, is surrounded by two asymmetric ferrimagnetic films with opposite collinear exchange configurations. The remanent magnetic textures obtained with this combination, where collinear exchange and magnetostatic interactions are competing in an in-depth asymmetric way, are discussed in the following sections.

2. Experimental methods

Single thin films and trilayers of RE-TM amorphous alloys have been deposited by co-sputtering of high purity Co (99.99 % atomic concentration) and Gd (99.9%) or Nd (99.9%) targets at an Ar working pressure of the order of ~ 10^{-3} mbar (base pressure ~ 10^{-8} mbar). The films have been grown on two types of substrates: Si(100) wafers with native oxide, and 50 nm thick silicon nitride membranes for Transmission X-ray Microscopy measurements, as discussed below. Protective cappings of Mo (10 nm thick) and buffer layers of Mo (10 nm thick) have been grown *in-situ* in two of the single films by sputtering. In the rest of the samples and trilayers, an Al capping (5 nm thick) to prevent oxidation has been deposited *ex-situ*, in another sputtering system, after a short period (~ minutes) of air exposure. The list of single films and trilayers prepared, with compositions indicated as Gd_xCo_{1-x}, is shown in the following table:

Sample	structure	capping	buffer
$Gd_{12}Co_{88}$	50 nm $Gd_{0.12}Co_{0.88}$	10 nm Mo	10 nm Mo
$Gd_{24}Co_{76}$	50 nm $Gd_{0.24}Co_{0.76}$	5 nm Al	no buffer
$Gd_{22}Co_{78}$	50 nm $Gd_{0.22}Co_{0.78}$	5 nm Al	no buffer
$Gd_{25}Co_{75}$	50 nm $Gd_{0.25}Co_{0.75}$	10 nm Mo	10 nm Mo
$40Gd_{12}/80Nd/40Gd_{25}$	40 nm $Gd_{0.12}Co_{0.88}$ / 80 nm $Nd_{0.17}Co_{0.83}$ / 40 nm $Gd_{0.25}Co_{0.75}$ / substrate	5 nm Al	no buffer
$40Gd_{25}/80Nd/40Gd_{12}$	40 nm $Gd_{0.25}Co_{0.75}$ / 80 nm $Nd_{0.17}Co_{0.83}$ / 40 nm $Gd_{0.12}Co_{0.88}$ / substrate	5 nm Al	no buffer
$40Gd_{12}/80Nd/40Gd_{24}$	40 nm $Gd_{0.12}Co_{0.88}$ / 80 nm $Nd_{0.17}Co_{0.83}$ / 40 nm $Gd_{0.24}Co_{0.76}$ / substrate	5 nm Al	no buffer
$40Gd_{24}/80Nd/40Gd_{12}$	40 nm $Gd_{0.24}Co_{0.76}$ / 80 nm $Nd_{0.17}Co_{0.83}$ / 40 nm $Gd_{0.12}Co_{0.88}$ / substrate	5 nm Al	no buffer
$80Gd_{24}/80Nd/80Gd_{12}$	80 nm $Gd_{0.24}Co_{0.76}$ / 80 nm $Nd_{0.17}Co_{0.83}$ / 80 nm $Gd_{0.12}Co_{0.88}$ / substrate	5 nm Al	no buffer
$80Gd_{12}/80Nd/80Gd_{24}$	80 nm $Gd_{0.12}Co_{0.88}$ / 80 nm $Nd_{0.17}Co_{0.83}$ / 80 nm $Gd_{0.24}Co_{0.76}$ / substrate	5 nm Al	no buffer

Table 1. List of the four single Gd-Co layers and six trilayers prepared, including the type of capping and buffer employed.

The magnetic properties of the samples have been characterized by a combination of several techniques. First, macroscopic Magneto-Optical Transverse Kerr effect (MOTKE) has been measured in a system equipped with a He cryostat. In addition, Variable Sample Magnetometry (VSM) has been carried out in a EV9 VSM system, from the company Microsense, in some trilayers. Microscopic images of the trilayers surface domain structure have been obtained by Magnetic Force Microscopy (MFM) measurements obtained with a microscope from the Nanotech company. Finally, element specific magnetic Transmission soft X-ray Microscopy (TXM) imaging at the Gd L_5 edge absorption energy has been performed at the microscope installed at the Mistral Beamline of the Alba synchrotron [26] on the trilayers grown on top of silicon nitride membranes. By using circularly polarized photons, and taking advantage of the X-ray Magnetic Circular Dichroism (XMCD) effect, microscopic images of the projection of the Gd magnetic moments along the direction of propagation of the photons have been acquired at different sample/photon beam orientations.

3. Results and discussion

As a first step in the design of the trilayers, MOTKE hysteresis loops of the four single layers indicated in the first rows of Table 1 have been measured with white light. MOTKE in the visible range of the spectrum is mainly sensitive to the Co magnetization [27] with probing depths of the order of few tens of nm [28]. This means that the sign of the saturation Kerr signal measured within a hysteresis loop contains information on the

magnetic subnetwork dominating the total magnetization of the RE-TM alloy. If Co is dominating, Co magnetic moments will align with the external magnetic field, and the Kerr signal at the positive saturation state of the loop will have positive sign. On the contrary, for alloys dominated by the Gd subnetwork, Gd moments will align with the external field, so that Co moments, which are responsible of the hysteresis loop sign, will point in opposite direction due to the negative Co-Gd exchange interaction, leading to negative Kerr signal at the positive saturation branch of the loops. This can be seen in Fig. 1, where the Kerr signal is depicted as a function of temperature. The figure indicates that at RT two of the samples are Co dominated, $Gd_{12}Co_{88}$ and $Gd_{22}Co_{78}$, whereas samples $Gd_{24}Co_{76}$ and $Gd_{25}Co_{75}$ are Gd dominated, as deduced from the sign of the loops. The figure indicates then that the transition between both regimes at RT takes place between 22 % and 24 % Gd atomic concentration, confirming that the compensation temperatures (where total magnetization vanishes) of these alloys are highly dependent on composition [10]. The 12 % Gd composition is dominated by Co in the whole range, whereas the 25 % and the 24 % are dominated by Gd in all the temperatures studied. On the contrary, the 22 % atomic Gd sample shows a transition from Co to Gd orientation at a compensation temperature of around 250 K. The corresponding coercive fields as a function of temperature can be seen in the inset of Fig. 1. This graph shows the characteristic increase around the compensation temperature, related with the change in Zeeman energy term due to the reduction of total magnetization when both subnetworks are close to compensation, in samples $Gd_{22}Co_{78}$ and $Gd_{24}Co_{76}$. Samples further away from the compensation composition at RT show the lowest values of coercive field, this effect being specially clear in $Gd_{12}Co_{88}$, with the highest Co concentration, which is an indication of its higher magnetization value.

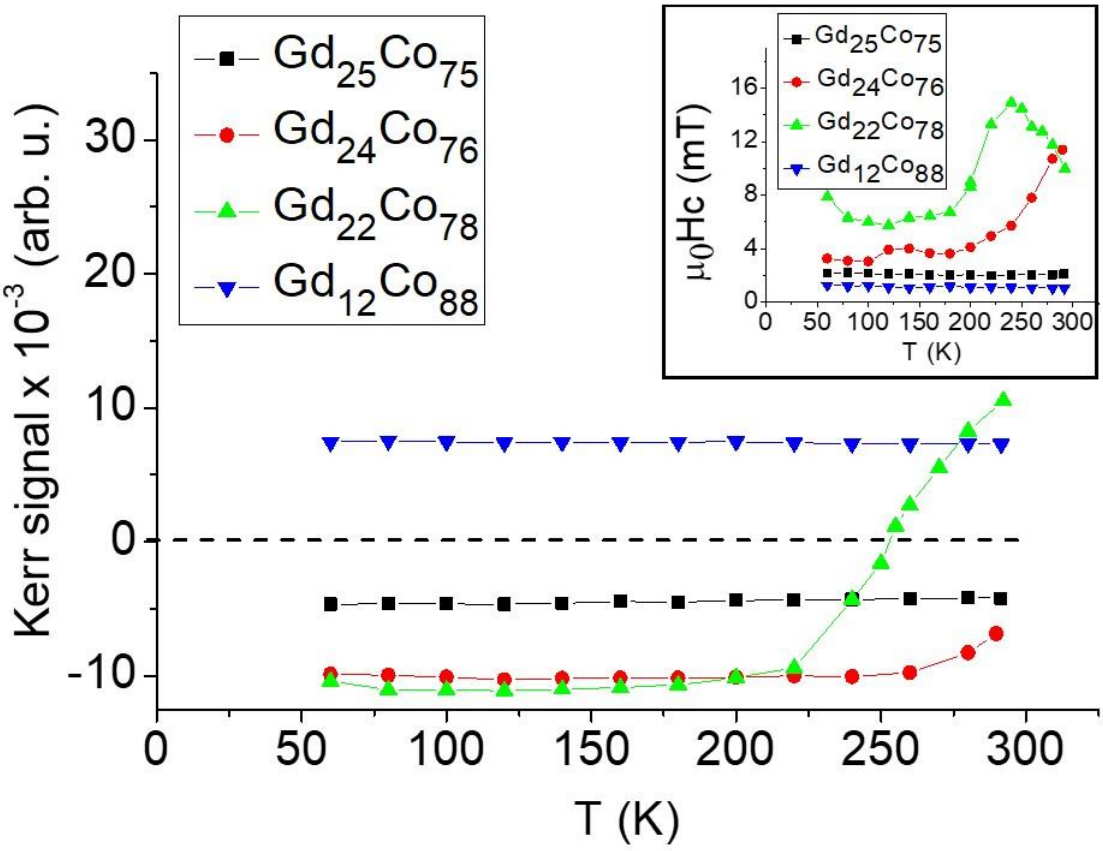

Figure 1. MOTKE signal at saturation field of single layers with different Gd concentrations; inset shows corresponding coercive field as a function of temperature.

This information has been taken into account in order to prepare trilayers where the competition between exchange, Zeeman and magnetostatic interactions is expected to stabilize magnetic singularities, selecting two compositions with opposite behaviors. The normalized MOTKE hysteresis loops are shown in Fig. 2 (a-b), which, according to the sign of the loops, correspond to relative orientations of the Co and Gd magnetic moments and total magnetization as indicated in the schematic arrows in the figures. Each of these layers have been placed below and above a central $NdCo_5$ layer with WPMA. The amorphous ferromagnetic layer of $NdCo_5$ is known to develop stripe domain patterns stable at remanence, above a certain thickness threshold of few tens of nanometers, due to the competition between perpendicular magnetic anisotropy and magnetostatic interactions [29]. If low anisotropy ferro or ferrimagnetic films are grown above or below this $NdCo_5$ central layer, the stripe domain pattern is transferred, by collinear exchange interactions between 3d transition metal atoms at the interfaces, to the surrounding layers, as it has been recently reported in Ni-Fe / Nd-Co / Gd-Co trilayers [14, 30]. In the outer layers, the canting out-of-plane average angle of the magnetization is smaller due to the minimization of the magnetostatic energy at the surfaces that leads to the formation of in-plane closure domains with alternate quirality [14].

According to these previous findings, in the trilayers studied in the present work, the exchange interaction between Co atoms is expected to transfer the stripe pattern domain structure of the central ferromagnetic Nd-Co layer to both external ferrimagnetic Gd-Co layers, where, in addition in-plane closure domains should be formed, as already mentioned. Furthermore, this exchange interaction coupling the 3d Co atoms across the trilayer thickness could lead to the stabilization of an in-depth domain wall for the magnetization at the interface between the Nd-Co ferromagnetic central layer and the Gd dominated ferrimagnetic layer. This is illustrated in the simplified scheme shown in Fig. 2 (c), where the domain wall is shown as a dashed yellow line.

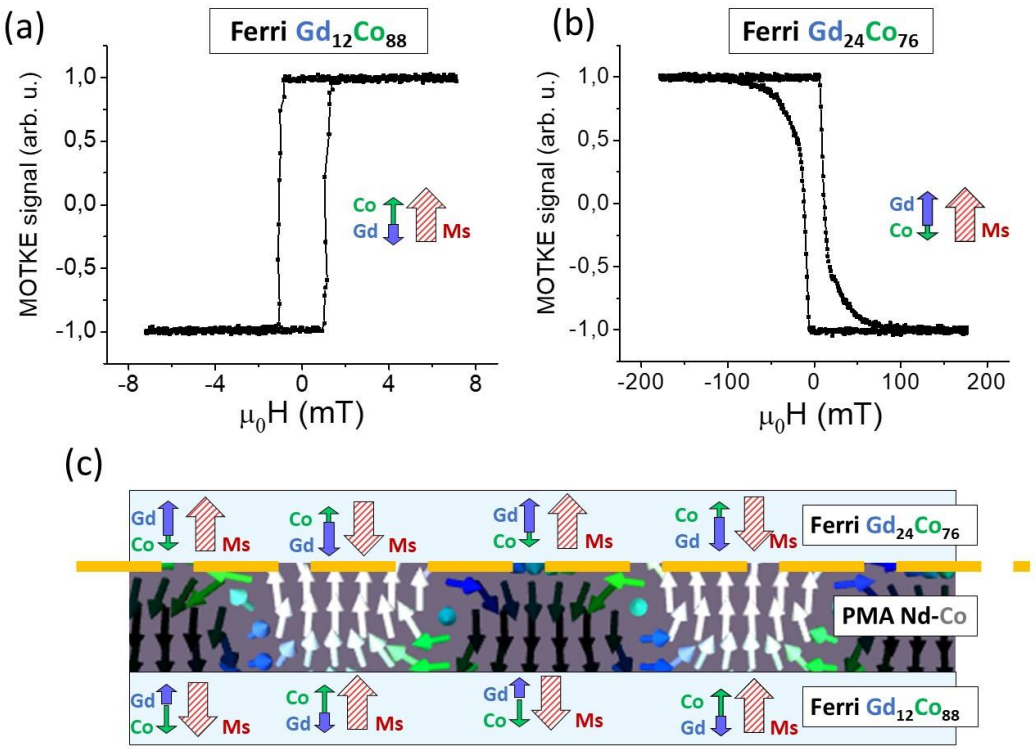

Figure 2. Normalized MOTKE hysteresis loops at RT for (a) sample $Gd_{12}Co_{88}$, with Co dominated concentration, and (b) sample $Gd_{24}Co_{76}$, with Gd dominated concentration; the arrows indicate the Gd and Co subnetworks magnetic moments, and total magnetization orientation (striped arrows); note the different scales of both horizontal axis; (c) cross section sketch of a magnetic trilayer, with a central $NdCo_5$ film surrounded by two ferrimagnetic GdCo alloys, corresponding to the concentrations indicated in panels (a) and (b), showing the typical up (white) and down (black) stripes. The dashed yellow line indicates the position of the in-depth domain wall.

With this general design, three families of trilayers have been grown with different thicknesses and compositions, as summarized in Table 1. In all cases the central $NdCo_5$ layer thickness has been fixed to 80 nm, which is an appropriate thickness to stabilize stripe domain patterns [29]. The composition of the Co rich layer has been fixed to 12 % atomic Gd for all the samples. With these parameters constant, we have grown two pairs of trilayers with two different compositions for the Gd rich layer, 25 % (samples $40Gd_{12}/80Nd/40Gd_{25}$ and $40Gd_{25}/80Nd/40Gd_{12}$) and 24 % (samples $40Gd_{12}/80Nd/40Gd_{24}$ and $40Gd_{24}/80Nd/40Gd_{12}$), where the thicknesses of all the Gd-Co layers has been set to 40 nm. The only difference between samples $40Gd_{12}/80Nd/40Gd_{25}$and $40Gd_{25}/80Nd/40Gd_{12}$ is the stacking sequence, which is reversed between them. The same holds for the second pair of trilayers $40Gd_{12}/80Nd/40Gd_{24}$ and $40Gd_{24}/80Nd/40Gd_{12}$, where the stacking sequence has been reversed too. Finally, a third pair of trilayers has been grown, $80Gd_{24}/80Nd/80Gd_{12}$ and $80Gd_{12}/80Nd/80Gd_{24}$, using 24 % atomic Gd concentration for the Gd rich ferrimagnetic layer but now increasing the thickness of all the Gd-Co layers to 80 nm. As in the other two pairs, the only difference between $80Gd_{24}/80Nd/80Gd_{12}$ and $80Gd_{12}/80Nd/80Gd_{24}$ is the stacking sequence.

In order to study the general macroscopic magnetic behaviour of these three pairs of trilayers, we have measured VSM hysteresis loops, as shown in Fig. 3, which correspond to in-plane applied magnetic fields in panels (a-c), and out-of-plane magnetic fields, panels (d-f). VSM loops have the advantage over MOTKE ones that probe the whole thickness of the samples. The hysteresis loops shown belong to one sample of each pair of trilayers. The first two samples have the same thicknesses, but different composition of the Gd rich layer, whereas the last two samples have the same composition in all the layers, but different thicknesses of the Co-Gd layers.

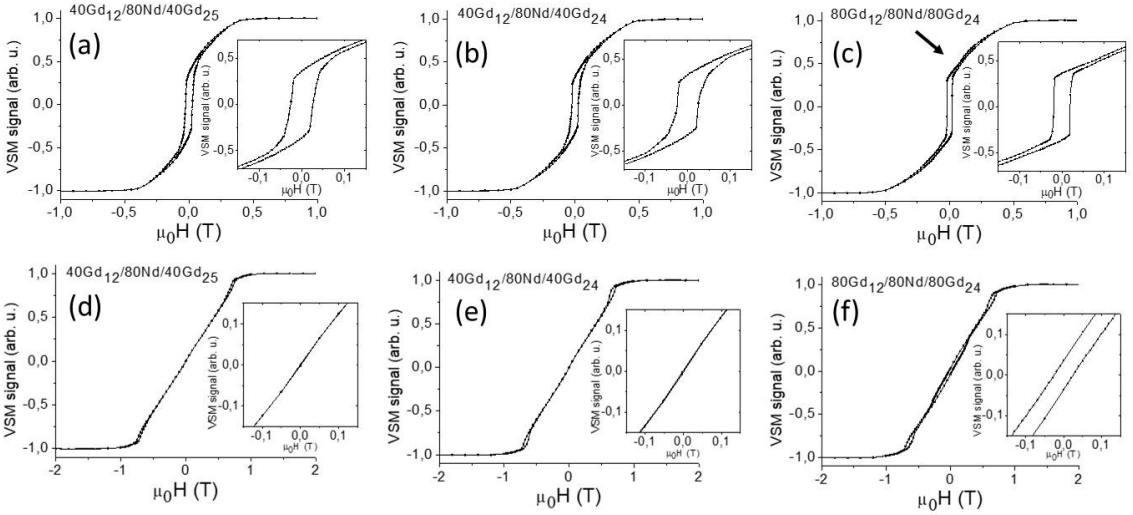

Figure 3. (a-c) in-plane and (d-f) out-of-plane normalized VSM hysteresis loops of trilayers (a) and (d) $40Gd_{12}/80Nd/40Gd_{25}$, (b) and (e) $40Gd_{12}/80Nd/40Gd_{24}$, and (c) and (f) $80Gd_{12}/80Nd/80Gd_{24}$. The arrow in panel (c) indicates a subtle change in the slope of the loop mentioned in the text. Insets show a more detailed view around coercivity.

The in-plane loops of all the samples (Fig. 3 (a-c)) show the transcritical shape consistent with the formation of stripe domain patterns at remanence [29]. The ratio of remanent magnetization (Mr) to saturation magnetization (Ms) for the samples ranges between 0.32 for $40Gd_{12}/80Nd/40Gd_{24}$ to 0.36 in samples $40Gd_{12}/80Nd/40Gd_{25}$ and $80Gd_{12}/80Nd/80Gd_{24}$. This indicates that the average out-of-plane component of the thicker sample is slightly smaller than the thinner with the same composition, most likely due to the increasing influence of the in-plane anisotropy of the Gd-Co layers. The coercive field reduces when increasing the trilayer thickness from 24.5 mT for sample $40Gd_{12}/80Nd/40Gd_{24}$ to 19.5 mT in $80Gd_{12}/80Nd/80Gd_{24}$. Interestingly, this last sample shows a subtle increase in slope when the external magnetic field is reduced from saturation to around 80 mT (see the arrow in Fig. 3 (c)) that is not observed in samples with only $NdCo_5$, pointing to a reversal mechanism with additional interactions than those happening in pure $NdCo_5$ films.

The corresponding out-of-plane loops (Fig.3 (d-f)) also show the shape related to stripe domains pattern formation, with saturation fields around 0.8-0.9 T, and almost zero remanent values due to the compensation of the out-of-plane components for the alternating stripes. However, again the thicker sample deviates from this general picture as it has a small hysteresis (Fig. 3 (f)) with remanence values different from zero (Mr/Ms ~ 0.04) and a tiny second jump in the loop with coercivities of around 0.27 T.

More insight on the magnetic behaviour of the trilayers is obtained by directly observing the domain structure using MFM measurements as those included in Fig. 4, that correspond to different magnetic states of the trilayers of each pair having the Gd rich layer on the top surface.

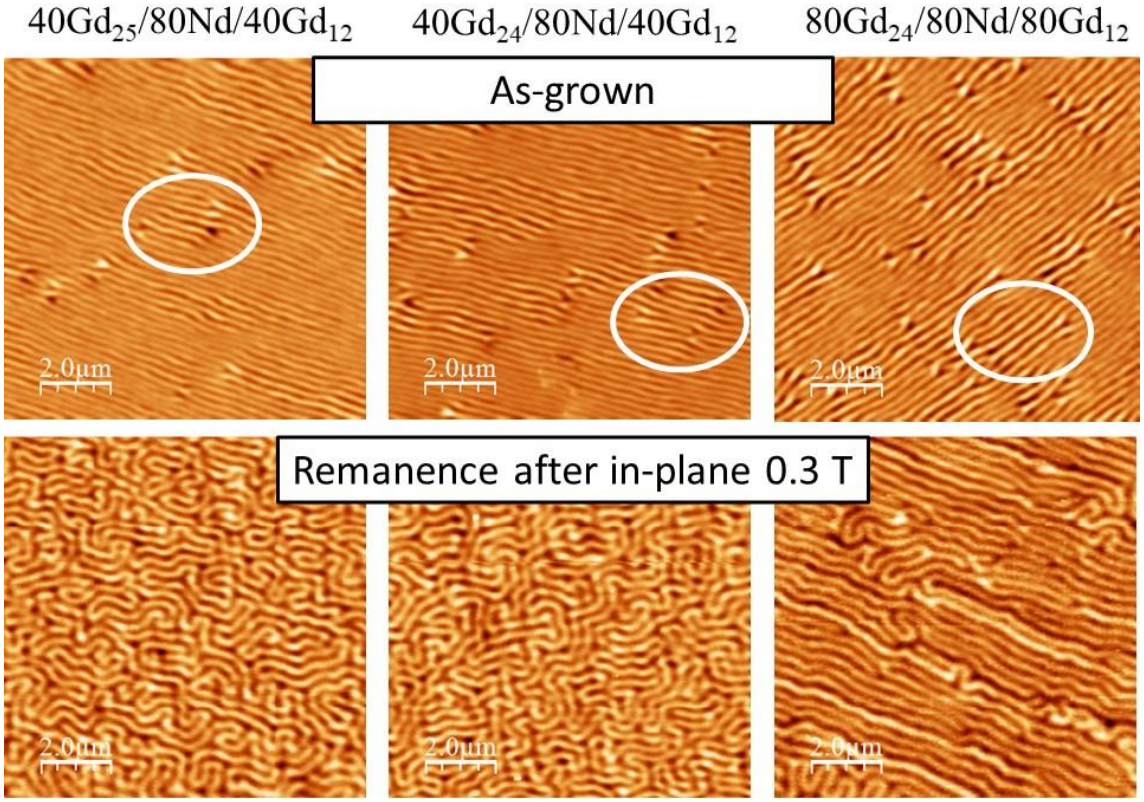

Figure 4. MFM measurements of three trilayers, corresponding to the top layer having Gd dominated magnetization. Each column of images refers to one sample. The first row has been measured at an as-grown magnetic state, whereas the second row are images obtained after applying an 0.3 T in-plane field and going back to remanence. Some areas with larger periodicity of the stripes have been marked by white ellipses in the first row of images.

The first row of Fig. 4, shows the as grown magnetic state of the trilayers, confirming the presence of stripe domains in all the trilayers, in agreement with the shape of the VSM loops discussed above. However, an unusual change in the periodicity of the stripes is observed for the three samples, which are not uniform, showing areas, few microns large, with shorter periodicities alternating with other areas with larger periodicities. More in detail, sample $40Gd_{25}/80Nd/40Gd_{12}$ changes the periodicities from around 250 nm to 190 nm, $40Gd_{24}/80Nd/40Gd_{12}$ from 270 nm to 210 nm, and the thicker trilayer $80Gd_{24}/80Nd/80Gd_{12}$ from about 280 nm to 210 nm, that is, a general reduction of around 20-25 % in stripe periodicity. These values have been directly estimated from the images making MFM signal profiles perpendicular to the stripes and counting the number of periods in a certain distance. As the periodicity of the stripes is the result of the minimization of the total magnetic energy of the system, the lack of homogeneity in the stripe domain periodicity is strong hint of the competition between magnetic interactions taking place in the trilayers. Furthermore, the images indicate the presence of dislocations, which are defects where the formation of magnetic singularities, like merons or Bloch

points [12,13,14], is expected. These dislocations are needed to accommodate the observed changes in periodicity, and they are accompanied by an enhancement of the MFM signal, more pronounced in the thicker sample, where the density of dislocations is larger, as it has the largest change in periodicity.

These differences between the thinner samples and the thicker one are also observed when the magnetic state is prepared by applying an in-plane magnetic field of 0.3 T and going to remanence, which correspond to the second row of Fig. 4. The images show that both thin trilayers develop marked maze domain patterns in contrast with the better aligned stripe pattern of the thicker trilayer. Furthermore, the MFM signal inside the stripes is not homogeneous, with sharp changes of intensity along the stripes, which show a trend to fragmentation, more pronounced in sample $40Gd_{24}/80Nd/40Gd_{12}$. The thicker sample, $80Gd_{24}/80Nd/80Gd_{12}$, even if it is better aligned than the previous, also shows a partial trend to formation of maze structures. In addition, in the thicker sample, very clear brighter / darker stripes, starting at dislocations or defects, are observed. These maze domains and changes in intensity observed in the trilayers are not usual in single $NdCo_5$ layers after applying in-plane fields. They suggest that partial in-depth magnetization reversals, leading to the formation of domains with non-homogeneous out-of-plane components, are taking place, as expected for the above mentioned competition between interactions.

Finally, TXM images of samples $40Gd_{24}/80Nd/40Gd_{12}$ and $80Gd_{24}/80Nd/80Gd_{12}$, with identical composition, but different thickness, have been acquired at the Gd L_5 edge, as shown in Fig. 5, at normal incidence in panels (a) and (c), and oblique incidence (rotation axis vertical) in panels (b) and (d). They correspond to a magnetic state prepared after applying out-of-plane demagnetizing loops starting at 2 T and cycling positive/negative fields with reducing amplitude down to zero. It is worth reminding that normal incidence images are sensitive to the out-of-plane component of the magnetization, whereas oblique incidence images are also sensitive to in-plane components. Black small circles correspond to 100 nm diameter gold nanoparticles spread into the sample for image alignment purposes. The first point to remark is that both samples have zigzag stripes, which could be a typical fingerprint of competing interactions, like those observed when stripes are superimposed to largest domains, or in the transition between parallel to field to perpendicular to field stripes [31]. A second relevant aspect is that normal incidence domain patterns of both samples have non-uniform contrasts that confirm the coexistence of different out-of-plane values of the magnetization. This effect is more clear in the thicker $80Gd_{24}/80Nd/80Gd_{12}$ sample (panel (c)) and can be associated to the non-zero value of Mr previously discussed in the corresponding VSM loop (Fig. 3 (f)).

When both samples are imaged at oblique incidence, a very complex domain structure is observed. In the thinner $40Gd_{24}/80Nd/40Gd_{12}$ sample, this domain pattern corresponds to a reversal of magnetization taking place through groups of few, or even single, stripes which, in addition, have different contrast values. Several intensity levels of white stripes, at least three, are observed, together with several levels of black ones. This may be explained by a combination of different in-plane and out-of-plane values of the magnetization. The areas corresponding to twisted transitions between these different intensity types of stripes, like those shown in the inset close to the brighter features, are places where Bloch points and in-depth domain walls are expected to be stabilized. In the thicker trilayer (Figs. 5 (c) and (d)), the reversed domains are less elongated and more equiaxial than in the thinner one, with domain borders that, in many occasions, follow the

places where the stripes make a sharp angle associated to the zigzags. Again, the areas in the oblique incidence image where different intensity levels are close to each other, or abrupt changes of intensity are observed along one single stripe, show complex magnetic textures where magnetic singularities are likely to be formed. Three examples of such places are highlighted with white circles in Fig. 5 (d). Understanding the details of such singularities requires a deeper characterization out of the scope of this work.

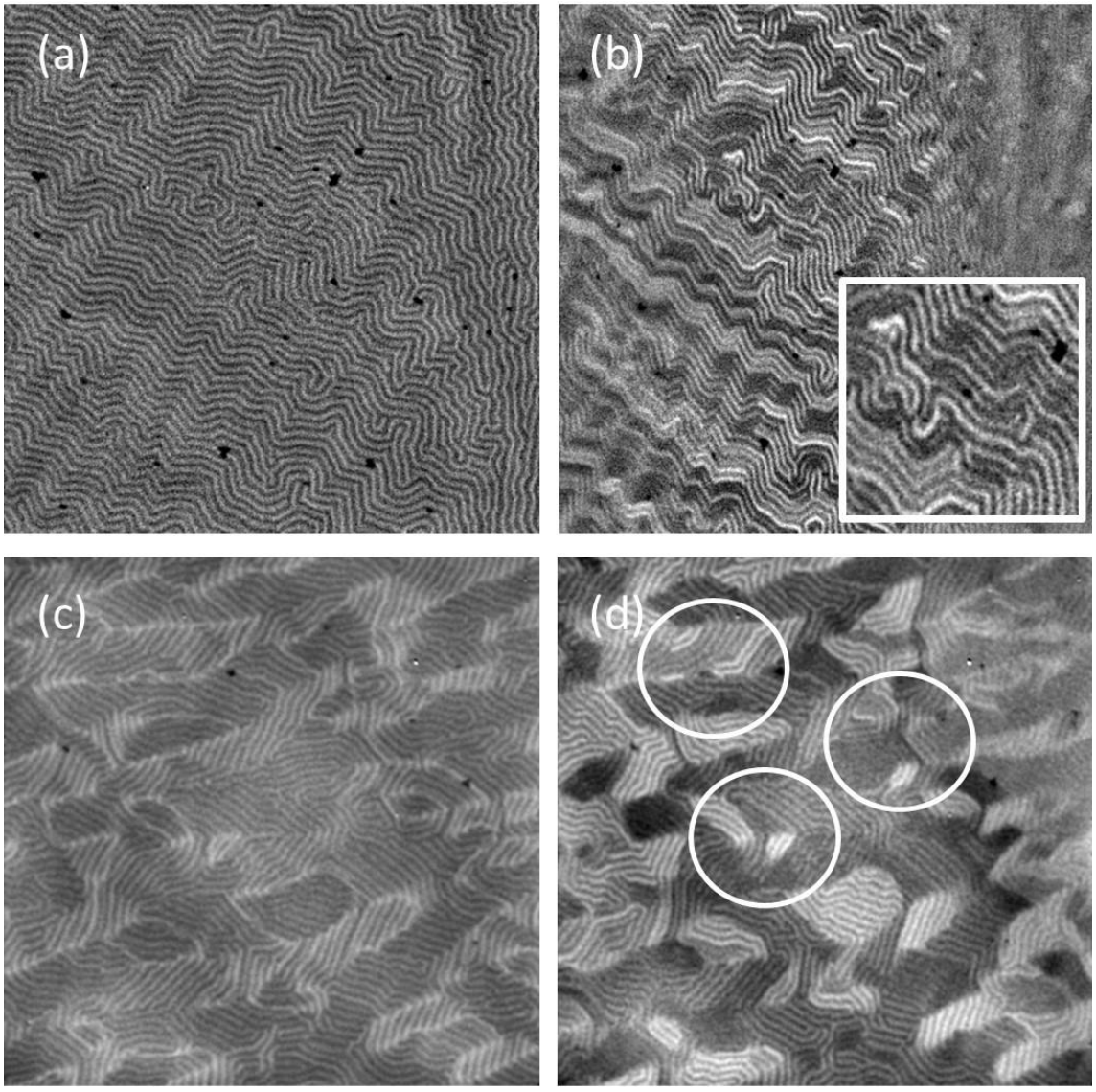

Figure 5. TXM image of samples $40Gd_{24}/80Nd/40Gd_{12}$ at (a) 0º and (b) -50º, and $80Gd_{24}/80Nd/80Gd_{12}$ at (c) 0º and (d) 30º after out-of-plane demagnetizing loop starting at + 2 T. The field of view corresponds to about 13 microns x 13 microns. The inset in panel (b) is an enlargement of the central part of the image and its field of view is 3.3 microns x 3.3 microns. Partial blurring in the left/right sides of panels (b) and (d) is due to depth of focus limitations when observation tilt angle increases.

4. Conclusions

In summary, the formation of stripe domains in magnetic trilayers of ferrimagnetic GdCo alloys with different compositions surrounding a central $NdCo_5$ ferromagnetic layer with perpendicular magnetic anisotropy has been confirmed by macroscopic VSM loops and MFM characterization. MFM shows characteristics of the trilayers not usually observed in single $NdCo_5$ layers: non-uniform periodicities of the stripe pattern, with areas several microns large where the periods change by about a 25 %, and non-uniform values of intensities along the stripes, with a trend to fragmentation of the stripes, maze domains formation, and changes in the intensity of stripes close to dislocations or defects after in-plain applied magnetic fields. These effects, combined with the dichroic contrasts observed in TXM images acquired at normal and oblique incidence, have allowed us to identify areas in the trilayers where partial reversal of the magnetization can be taking place leading to complex magnetic textures, stabilized by the competition between exchange, magnetostatic, and Zeeman interactions.

Acknowledgments

This work was supported by Spanish MINECO under Project No. FIS2016-76058 (AEI/FEDER, UE), and Spanish MCI under Project No. PID2019-108075RB-C32/AEI/10.13039/501100011033. These experiments were performed at the MISTRAL beamline at ALBA Synchrotron with the collaboration of ALBA staff. David Martínez Blanco, from Servicios Científico-Técnicos (Unidad de medidas magnéticas / RMN sólidos) Universidad de Oviedo, is acknowledged for VSM measurements. A. H.-R. acknowledges the support from European Union's Horizon 2020 research and innovation program under Marie Skłodowska-Curie grant ref. H2020-MSCA-IF-2016-746958. J. H. acknowledges the support from Vicerrectorado de Investigación of Universidad de Oviedo (Plan de Apoyo y Promoción de la Investigación 2020).

Bibliography

[1] A. Fernández-Pacheco, Robert Streubel, Olivier Fruchart, Riccardo Hertel, Peter Fischer, Russell P. Cowburn, Nat. Comm. 8 (2017) 15756.
[2] Claire Donnelly, Manuel Guizar-Sicairos, Valerio Scagnoli, Sebastian Gliga, Mirko Holler, Jörg Raabe2 and Laura J. Heyderman, Nature 547 (2017) 328.
[3] Katharina Witte, Andreas Späth, Simone Finizio, Claire Donnelly, Benjamin Watts, Blagoj Sarafimov, Michal Odstrcil, Manuel Guizar-Sicairos, Mirko Holler, Rainer H. Fink, and Jörg Raabe, Nano Lett. 20 (2020) 1305.
[4] A. Hierro-Rodriguez, C. Quirós, A. Sorrentino, L. M. Alvarez-Prado, J. I. Martín, J. M. Alameda, E. Pereiro, M. Vélez, and S. Ferrer, Nat. Comms. 11 (2020) 6382.
[5] Charudatta Phatak, Amanda K. Petford-Long, and Marc De Graef, Phys. Rev. Lett. 104 (2010) 253901.
[6] Shilei Zhang, Gerrit van der Laan, Jan Mu¨ ller, Lukas Heinen, Markus Garst, Andreas Bauer, Helmuth Berger, Christian Pfleiderer, and Thorsten Hesjedal, PNAS 115 (2018) 6386.
[7] P. Chaudhari, J.J. Cuomo, and R.J. Gambino, Appl. Phys. Lett. 22 (1973) 337.
[8] Henryk K. Lachowicz, IEEE Trans. Magnet. 20 (1984) 1417.
[9] P. Hansen, in *Handbook of Magnetic Materials*, edited by K. H. J. Buschow Elsevier, Amsterdam, 1991, Vol. 6, p. 289.

[10] R. Morales, J. I. Martín, and J. M. Alameda, Phys. Rev. B 70 (2004) 174440.
[11] A. Hubert and R. Schafer. Magnetic Domains: The Analysis of Magnetic Microstructures (Springer-Verlag, Berlin, 1998), section 5.5.5.A.
[12] C. Blanco-Roldán, C. Quirós, A. Sorrentino, A. Hierro-Rodríguez, L.M. Álvarez-Prado, R. Valcárcel, M. Duch, N. Torras, J. Esteve, J.I. Martín, M. Vélez, J.M. Alameda, E. Pereiro and S. Ferrer, Nat. Comm. 6 (2015) 8196.
[13] M. Ezawa, Phys. Rev. B 83 (2011) 100408(R).
[14] A. Hierro-Rodriguez, C. Quirós, A. Sorrentino, C. Blanco-Roldán, L. M. Alvarez-Prado, J. I. Martín, J. M. Alameda, E. Pereiro, M. Vélez, and S. Ferrer, Phys. Rev. B 95 (2017) 014430.
[15] A. Hierro-Rodriguez, C. Quirós, A. Sorrentino, R. Valcárcel, I. Estébanez, L. M. Alvarez-Prado, J. I. Martín, J. M. Alameda, E. Pereiro, M. Vélez, and S. Ferrer, Appl. Phys. Lett. 110 (2017) 262402.
[16] A. D. Naylor, G. Burnell, and B. J. Hickey, Phys. Rev. B 85 (2012) 064410.
[17] B. Sanyal, C. Antoniak, T. Burkert, B. Krumme, A. Warland, F. Stromberg, C. Praetorius, K. Fauth, H.Wende, and O. Eriksson, Phys. Rev. Lett. 104 (2010) 156402.
[18] R. Hasegawa, J. Appl. Phys. 46 (1975) 5263.
[19] C. Blanco-Roldán, Y. Choi, C. Quirós, S. M. Valvidares, R. Zarate, M. Vélez, J. M. Alameda, D. Haskel, and J. I. Martín, Phys. Rev. B 92 (2015) 224433.
[20] J. Brandão, D. A. Dugato, M. V. Puydinger dos Santos, and J. C. Cezar, ACS Appl. Nano Matter 2 (2019) 7532.
[21] Lucas Caretta, Maxwell Mann, Felix Büttner, Kohei Ueda, Bastian Pfau, Christian M. Günther, Piet Hessing, Alexandra Churikova, Christopher Klose, Michael Schneider, Dieter Engel, Colin Marcus, David Bono, Kai Bagschik, Stefan Eisebitt and Geoffrey S. D. Beach, Nat. Nanotech. 13 (2018) 1154.
[22] Seonghoon Woo, Kyung Mee Song, Xichao Zhang, Yan Zhou, Motohiko Ezawa, Xiaoxi Liu, S. Finizio, J. Raabe, Nyun Jong Lee, Sang-Il Kim, Seung-Young Park, Younghak Kim, Jae-Young Kim, Dongjoon Lee, OukJae Lee, Jun Woo Choi, Byoung-Chul Min, Hyun Cheol Koo and Joonyeon Chang, Nat. Comm. 9 (2018) 959.
[23] Kab-Jin Kim, Se Kwon Kim, Yuushou Hirata, Se-Hyeok Oh, Takayuki Tono, Duck-Ho Kim, Takaya Okuno,Woo Seung Ham, Sanghoon Kim, Gyoungchoon Go, Yaroslav Tserkovnyak, Arata Tsukamoto, Takahiro Moriyama, Kyung-Jin Lee and Teruo Ono, Nat. Mater. 16 (2017) 1187.
[24] S. Mangin, M. Gottwald, C-H. Lambert, D. Steil, V. Uhlíř, L. Pang, M. Hehn, S. Alebrand, M. Cinchetti, G. Malinowski, Y. Fainman, M. Aeschlimann, and E. E. Fullerton, Nat. Mat. 13 (2014) 286.
[25] Andrada-Oana Mandru, Oğuz Yıldırım, Riccardo Tomasello, Paul Heistracher, Marcos Penedo, Anna Giordano, Dieter Suess, Giovanni Finocchio and Hans Josef Hug, Nat. Comm. 11 (2020) 6365.
[26] A. Sorrentino, J. Nicolas, R. Valcarcel, F. J. Chichon, M. Rosanes, J. Avila, A. Tkachuk, J. Irwin, S. Ferrer, and E. Pereiro, J. Synchr. Radiat. 22 (2015) 1112.
[27] K. Sato and Y. Togami, J. Magn. Magn. Mater. 35 (1983) 181.
[28] C. Dehesa-Martínez, L. Blanco-Gutiérrez, M. Vélez, J. Díaz, L. M. Alvarez-Prado, and J. M. Alameda, Phys. Rev. B 64 (2001) 024417.
[29] A. Hierro-Rodriguez, G. Rodríguez-Rodríguez, J. M. Teixeira, G. N. Kakazei, J. B. Sousa, M. Vélez, J. I. Martín, L. M. Alvarez-Prado and J. M. Alameda, J. Phys. D: Appl. Phys. 46 (2013) 345001.
[30] C. Quiros, A. Hierro-Rodriguez, A. Sorrentino, R. Valcarcel, L. M. Alvarez-Prado, J. I. Martín, J. M. Alameda, E. Pereiro, M. Vélez, and S. Ferrer, Phys. Rev. Appl. 10 (2018) 014008.

[31] A. Hubert and R. Schafer. Magnetic Domains: The Analysis of Magnetic Microstructures (Springer-Verlag, Berlin, 1998), sections 3.7.2.C and 5.4.2.B.